SCOPE | SAUDI INTERNATIONAL CONFERENCE ON NUCLEAR POWER ENGINEERING

Proceedings of SCOPE
13-15 Nov. 2023 – KFUPM
Paper 23061

Numerical Investigation of the Breath Figure Spot Characteristics in a Jet Impingement Condensation Process

Ali Alshehri [1,2]
[1]Mechanical Engineering Department, King Fahd University of Petroleum and Minerals (KFUPM),Dhahran 31261, Saudi Arabia.
[2]Interdisciplinary Research Center for Renewable Energy and Power Systems, King Fahd University of Petroleum and Minerals (KFUPM), Dhahran 31261, Saudi Arabia.
Email: alshehri@kfupm.edu.sa

Abstract – Condensation is a pivotal process in several applications including the nuclear industry. Its application in the nuclear industry includes but not limited to power generation, preventing loss-of-coolant accidents, and mitigating over-pressurizing of the containment building. The presence of non-condensable gases (NCG) significantly reduces the condensation heat transfer, causing several safety concerns. A better understanding of the physics of the accumulation of NCG owing to condensation leads to the design of efficient heat removal and better coolant recovery mechanisms. In a recent study, jet impingement condensation (JIC) was reported as an excellent technique for achieving high condensation rates owing to the improved thinning of the diffusion boundary layer associated with the accumulation of NCG near the liquid-vapor interface. Designing an optimal JIC system requires understanding its physics at varying parameters, such as jet size, jet-to-surface distance, jet speed, jet-to-surface temperature/concentration difference, and environmental temperature/concentration. In this study, we present a numerical model to investigate the influence of several parameters on the initial stages of the condensation process. We look mainly at modeling the Breath Figure (BF) spots, which are defined as the effective areas at which condensation occurs. The numerical model developed in this work was validated against experimental work and semi-analytical solution on a single round jet issuing from a tube at a prescribed temperature, NCG concentration, and flow rate. This paper investigates the flow, temperature, and concentration fields to gain better understanding of the BF appearance. We further show how the velocity, temperature, and concentration profiles are characterized by unique power laws in four different regions. The four different regions are distinguished by a unique behavior of how the maximum velocity in the hydraulic boundary layer varies with the radial location. Our model provides an effective numerical tool for better understanding the physics of efficient condensation in the presence of NCG.

Keywords: Phase change, Condensation, non-condensable gases, Thermal-hydraulics.

I. Introduction

Condensation is a fundamental process in many industrial applications, including the nuclear industry. In nuclear power plants, condensation is used to convert steam into water, which can then be recycled for use in the power generation process. Additionally, condensation process is essential for maintaining the proper functioning of the power plant. If the steam is not condensed efficiently, the water level in the steam generators can drop, which can expose the fuel rods to air and cause overheating and damage to the reactor core. In extreme cases, this can lead to a nuclear accident. In addition to its critical role in normal operation, condensation can also play a crucial role in accident scenarios in nuclear power plants. In the event of a loss-of-coolant accident (LOCA) or a steam line break, large amounts of steam can be released into the

containment building, increasing the pressure and temperature inside. To prevent over-pressurization, the containment building may need to be vented. In some cases, this venting can be accomplished through the use of a condenser. The steam is directed to the condenser, where it is condensed back into liquid, reducing the pressure and temperature inside the containment building. Furthermore, the presence of non-condensable gases (NCG), such as helium and hydrogen, can significantly impact the efficiency of condensation. These gases can accumulate in steam generators and other components, reducing the amount of heat transfer and increasing the risk of corrosion and damage to the equipment. As a result, understanding and managing the behavior of NCG during condensation is a crucial concern for the nuclear industry, and significant research has been conducted to optimize condenser performance in the presence of these gases [1].

The high convective heat and mass transfer coefficients associated with impinging jets have been successfully utilized in several industrial applications, such as drying processes, electronic cooling, and cooling of turbine blades, to name a few. Most recently, jet impingement condensation has been reported as an excellent means for high condensation rates due to the improved thinning of the diffusion boundary layer associated with the accumulation of NCG near the liquid-vapor interface. This allows for designing compact condensers with improved efficiencies compared to conventional heat-exchanger condenser designs [2]–[4].

Ji et al. [3] discussed the use of the steam jet method to improve the condensation heat transfer performance in the presence of NCG. The study involved designing an experimental facility where steam was injected vertically into a single aluminum tube. The results of the experiment showed that the steam jet injection method can effectively improve condensation performance, especially in the case of an accident where a large amount of NCG flows into the condenser.

Ji et al. [4] explored the impact of NCG on condensation heat transfer and compared the effectiveness of super-hydrophobic surfaces along with steam jet injection - in reducing NCG impact. The study was conducted using a test chamber with two test tubes, one with a non-modified surface and the other with a super-hydrophobic surface, to evaluate their performance under the same conditions. The results showed that the steam jet injection method yielded a steady heat transfer enhancement ratio. The paper provides insights into the methods that can be used to improve condensation heat transfer in the presence of NCG.

Alshehri et al. [5] investigated the use of jet impingement technique in improving the condensation rates under humid environment that is characterized by a significant NCG concentrations. The authors presented an experimental design that utilized a single jet of humid air impinging on a condenser surface. Results showed a substantial improvement in the condensation rates compared to state-of-the-art condensers. They experimentally evaluate the mass transfer coefficient using an optical method of observing the growth and departure of condensate droplets near the impingement region.

Alshehri and Kavehpour [6] explored the phenomenon of Breath Figure (BF) spot which appears when a jet of humid air is directed towards a cooled surface below the dew point. The authors illustrated that a BF spot generated on a cooled surface is a manifestation of a recovery concentration and provided scaling analysis and semi-analytical solutions to quantify the dimensions of the BF spots at varying conditions. The paper concluded that BF spots are important to quantify as they define the effective areas over which condensation takes place. The semi-analytical solution provided included several assumptions, such as the self-similar velocity, and concentration profiles within the boundary layer.

In this paper, a comprehensive numerical analysis is presented to quantify the dimensions of the BF spot. Moreover, the flow, thermal, and concentration fields are examined in detail to gain a better understanding of the underlying mechanisms governing the occurrence of the BF spot. The numerical model developed for this study was validated experimentally, and it is deemed an indispensable tool for further investigating the condensation process under jet impingement conditions.

II. Numerical Modelling

The geometrical configuration and boundary conditions of the problem are illustrated in **Figure 1Figure 2**. The problem at hand concerns a stream of humidified air with a vapor mass concentration ($\omega_{v,j}$) and temperature (T_j) issuing from a tube that has a diameter (D) with a mean velocity of (v_j). The length of the tube is such that a fully developed flow is achieved (L = 20D). The exit of the tube is at a standoff distance (H) from the condenser surface that extends beyond the

jet impingement region ($r = 50D$). The jet of humid air exits into a stagnant humid air ambient at a temperature (T_∞) and vapor mass concentration ($\omega_{v,\infty}$). After the jet impinges on the surface, it exits through the outlet boundaries which assume an ambient temperature (T_∞), ambient pressure (P_∞), and ambient vapor mass fraction ($\omega_{v,\infty}$) for the back-circulating and entrained flow of air. The system can be simplified to an axisymmetric domain as illustrated in **Figure 1**. The variation in variables along the angular axis (θ) is assumed to be negligible.

Alshehri et al. [2] numerically studied the condensation problem over a vertical flat plate in the presence of NCG and concluded that the thermal resistance of the diffusion layer is much higher than that of the condensate film/droplets for a high concentration of NCG. Therefore, the type of condensation that takes place on the surface, i.e. film or dropwise, is irrelevant in this work. Additionally, because the current work concerns the BF spot modelling, which takes place immediately after the jet impinges on the surface, we assume that the BF spot dimensions will not be affected significantly by the presence of condensate at the surface. Alshehri and Kavehpour [6] showed that the experimental observation of the BF spot dimensions can be semi-analytically modelled by assuming that the surface has a zero-mass transfer of vapor, i.e. $\partial\omega_v/\partial z = 0$. It has also been observed that the vapor mass fraction on the surface varies from a maximum in the impingement region to a minimum in a further radial distance in the case of an adiabatic wall condition. This results in a reduction of the dew point on the surface from the center to the edge of the condenser surface. As the surface is cooled to a specified temperature, the BF spot takes a unique dimension corresponding to the dew point at the periphery of the BF spot [6].

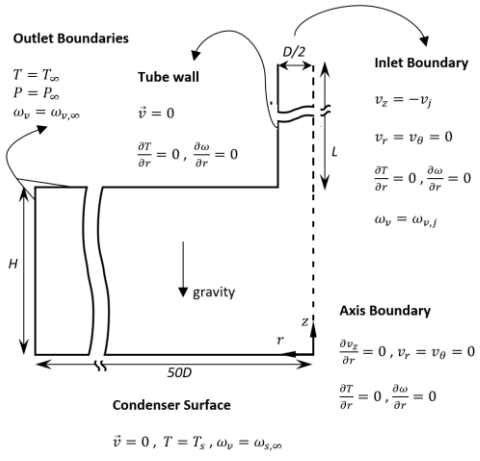

Figure 1: Physical model illustrating a simplified 2D axisymmetric domain with boundary conditions depicted.

II.A. Governing Equations

The mass, momentum, and energy conservation equations are solved for the vapor-air mixture domain, while the species mass conservation equation is solved for the water vapor. The continuity equation is given in general as

$$\frac{\partial \rho_g}{\partial t} + \nabla \cdot (\rho_g \vec{v}) = 0 \tag{1}$$

The momentum conservation is written as

$$\frac{\partial}{\partial t}(\rho_g \vec{v}) + \nabla \cdot (\rho_g \vec{v}.\vec{v}) = -\nabla P + \nabla \cdot \bar{\bar{\tau}} + \rho_g \vec{g} \tag{2}$$

The energy conservation is written as

$$\frac{\partial}{\partial t}(\rho_g E) + \nabla \cdot \left(\vec{v}.(\rho_g E + P)\right) = \nabla \cdot \left(k_g \nabla T - \sum_j h_j \vec{J}_j\right) \tag{3}$$

The water vapor transport equation is written as

$$\frac{\partial \rho_j}{\partial t} + \nabla \cdot (\rho_j \vec{v}) = -\nabla \cdot \vec{J}_j \tag{4}$$

By neglecting pressure work and kinetic energy, we can state that the total energy is approximately equivalent to the total enthalpy of the vapor-air mixture. Total enthalpy is a mass-weighted average of air and water vapor enthalpies. The enthalpy of the species is written as follows.

$$h_j = \int_{T_{ref}}^{T} c_{p,j}\, dT \tag{5}$$

The term ($\vec{J}_j$) in Eq. 3 and Eq. 4 refers to the diffusive mass flux of each species, which is given by Fick's law.

$$\vec{J}_j = -D_{j,i} \nabla \rho_j \tag{6}$$

The shear-stress transport (SST) k-ω model was used to simulate the jet impingement problem. Details of the transport equation of the turbulent kinetic energy and the specific dissipation rate can be found in the FLUENT theory guide [7]. The SST k-ω model was reviewed to give acceptable results in jet impingement problems [8].

In the previous equations, all thermophysical properties were taken as state-variable dependent, using the kinetic theory for the gas mixture. The Lennard-Jones characteristic length/energy ratios are 3.711/78.6 Å/K and 2.605/572.4 Å/K for air and water vapor, respectively. The Lennard-Jones potential parameters used can be found in standard kinetic theory textbooks [9]. The vapor mass concentration at any given temperature was found assuming saturated air. Air is treated as a single phase; therefore, modelling the mixture of water vapor and air is assumed as a binary gas mixture. Furthermore, the ideal gas law holds for the vapor-gas mixture. This limits the model to temperatures and pressures where the law is applicable. In a humid ambient environment, as in our work, this assumption is applicable [2]. Furthermore, the thermal resistance of the gas diffusion layer is much greater than that of the condensate droplets/film. This assumption has been shown to be valid, especially at high NCG concentrations [2]. Lastly, the liquid-gas interface is assumed to introduce a no-slip boundary condition in the gas mixture [2].

II.B. Grid Independence Test

An extreme case was simulated where the jet speed is very high, resulting in a Reynolds number ($Re = v_j D/\nu = 10{,}000$). A jet temperature that is equal to the ambient temperature of 300 K. It is assumed that air is saturated with water vapor at both the inlet and outlet boundary conditions ($\omega_{v,j} = \omega_{v,\infty} = 0.02197$ kg-vapor to the total mass of vapor-air mixture). It was also assumed that the turbulence intensity at the inlet condition is 5% with a turbulent viscosity ratio of 10. Varying the turbulent parameters did not affect the final results; however, they are kept at the mentioned values throughout the simulations in this work. The temperature of the condensation wall was 290 K. ANSYS Fluent was used to solve the governing equations using a coupled pressure-volume scheme with second order upwind discretization for all the parameters. The SST k-omega turbulent model was used in this work as it has been used in several jet impingement computations and is recommended for its versatility in simulation of several complex fluid flow problems [8]. The results were accepted when residuals fell below 10^{-7} and the mass fluxes at the inlet and outlet boundary conditions reached a steady state value.

The Y-plus value at the wall at different number of mesh elements along the radial direction was checked. The Y-plus values are close to unity with 160,000 elements and higher. This indicates that number of elements are sufficient to capture the turbulent boundary layer property variations. Furthermore, the Y-plus value peaks at a certain distance in the radial direction. This distance coincides with the region between the impingement region and the wall jet region. The grid-independent solution is obtained by making sure that the velocity profile is captured very well at this indicated radial direction.

Figure 2 depicts the velocity profiles along a normal line to the condensation wall using different numbers of elements. The profiles depicted were chosen at radial locations that are close to where the maximum Y-plus values were attained, that is, r / D = 0.6. It is evident that the highest element size of 360,000 captures the most accurate profile. This is clear due to the several points inside the boundary layer; to be specific, there are 13 points within 0.2 mm. The smallest number of elements of 6400 shows a pronounced deviation. Simulations with 160,000 elements have a comparable accuracy to that of 360,000, yet the maximum Y-plus value is slightly greater than unity. Therefore, for better accuracy and because computational time is not a concern for this work, we opted for the maximum number of elements in this study.

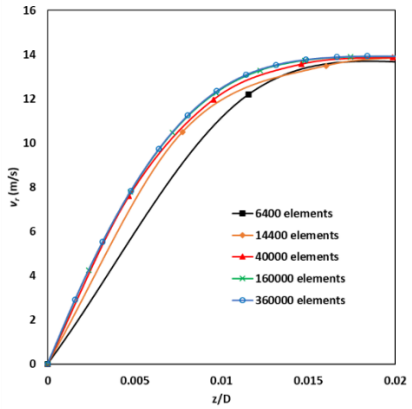

Figure 2: Grid-independent test showing the radial velocity profile near the wall at r/D=0.6.

II.C. Model Validation

To validate our model, we compare the results with the experimental work of Alshehri et al. [6]. The experimental conditions are summarized in **Table I**. Details of the experimental work can be reviewed in the cited manuscript.

Table I: Summary of the experimental work of Alshehri and Kavehpour validation test [6].

Variable	H/D	Re	$T_j = T_\infty$	RH_∞	RH_j
Value	4.5	4130	295 K	20 %	95 %

Figure 3 shows the comparison of the experimental data and the current numerical model. In the figure, the variation of the dimensionless vapor mass fraction on the wall as a function of dimensionless radial distance is depicted. The agreement between the two results is clear with a maximum deviation of 15% very close to the center of the impingement region. This error decreases with higher radial distances. Therefore, the results of our model is expected to give a suitable estimate of the vapor mass fraction on the surface.

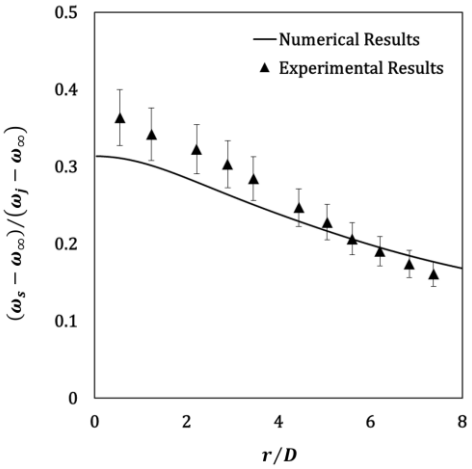

Figure 3: Validation of the model against the experimental data [6].

III. RESULTS AND DISCUSSION

To understand the appearance of the BF spots on condenser surfaces under jet impingement of humid air, we further quantify the flow, thermal, and species fields. Furthermore, we inspect the accuracy of the analytical model developed by Alshehri and Kavehpour [6]. The importance of quantifying the BF spot dimensionality is to optimize the placement of jet nozzles in a scaled-up array of jets. The BF spots were defined as the area within which condensation takes place [6]. Therefore, having a condenser surface area greater than the BF spot coverage area is unnecessary.

III.A. Flow field characterization

Figure 4A illustrates the contours of the radial velocity of the gas mixture in the computational domain. The jet exits the tube as a fully developed turbulent flow with negligible radial velocity. As the flow enters the ambient domain, it expands with a decaying velocity profile in the radial direction. Near the exit, a negative radial velocity is observed indicating an entrainment of the ambient gas within the expanding jet cone. The expanding jet then impinges on the condenser surface and the flow turns into the radial direction. The maximum radial velocity is observed to take place at a certain radial distance. As air travels in the radial direction, its velocity decreases, and a boundary layer forms near the condenser surface. The maximum radial velocity in the simulated case ($v_j = 20.24$ m/s) is almost 0.28 times the jet inlet velocity.

A

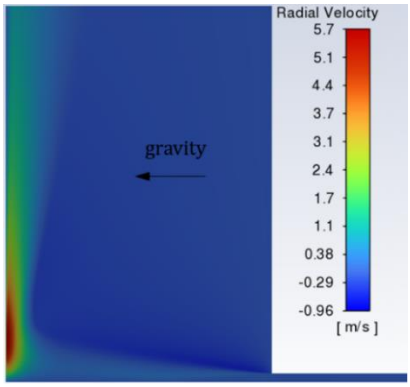

B

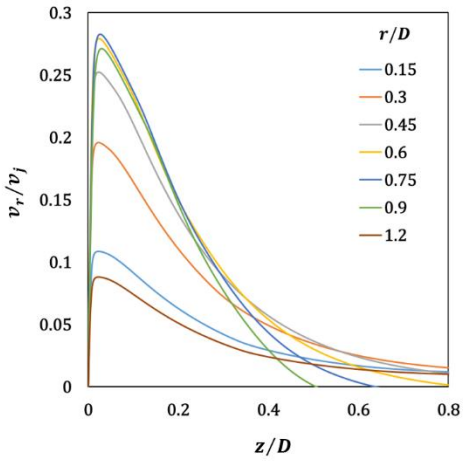

C

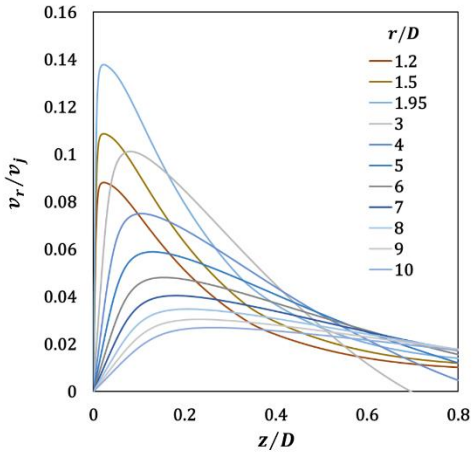

Figure 4: (**A**) Radial velocity contours near the impingement region for the case of Re = 4130 (v_j=20.24 m/s), (**B** and **C**) Velocity distribution within the boundary layer at different radial locations for the case of Re = 4130 (v_j=20.24 m/s).

Figure 4B and **C** show the velocity profiles at different radial locations within the boundary layer as a function of the axial location. The velocity profile is characterized by a maximum radial velocity at a certain axial location then a decay to an approximately zero velocity outside the boundary layer. As the radial location changes from $0.15D$ to $0.75D$ the maximum radial velocity increases from $0.11\,v_j$ to $0.28\,v_j$, respectively. At higher radial locations, the maximum velocity starts to decrease sharply. From a radial location of $0.75D$ to $1.2D$, the maximum radial velocity decreases to $0.1v_j$. The further increase of the radial location is characterized by yet an increase in the maximum radial velocity until a radial location of $1.95D$ after which the maximum radial velocity starts to decrease again. Therefore, we conclude that there are four distinct regions within which the velocity profiles take different shapes and characteristics. This is further illustrated in **Figure 5A,** which shows the variation of the dimensionless maximum radial velocity as a function of the dimensionless radial location. The first region lies within $0.15D$ to $0.75D$ within which a sudden increase in v_{max}/v_j value after which a sudden drop in v_{max}/v_j occurs to $1.2D$. The aforementioned regions are very narrow and required more points to clearly observe the correlation between v_{max}/v_j and r/D. BF spots observed in the experimental work of Alshehri and Kavehpour were on higher radial locations, therefore, it suffices to point these regions out in this work. The following region is characterized by a gradual increase in v_{max}/v_j from $1D$ to $2D$. The power law governing this increase is indicated in **Figure 5A** as $v_{max}/v_j \sim (r/D)^{0.93}$ with a leading constant of 0.074. The last observed region is indicated by a decrease v_{max}/v_j with the radial location with a power law of $v_{max}/v_j \sim (r/D)^{-1.1}$ with a leading constant of 0.34. The analytical derivation of Alshehri and Kavehpour [6] was based only on the final region, see Eq. 10 in the cited manuscript.

Figure 5B shows the location of the maximum radial velocity profile at different radial locations. It is clear that the maximum velocity occurs at a constant axial location within the boundary layer for the first three regions discussed above. The location of the maximum radial velocity starts to increase only for the final region characterized by a distinct power law of $\delta_{max}/D \sim (r/D)^{0.97}$ with a leading constant of 0.03. This result is consistent with Eq. 11 in Alshehri and Kavehpour [6].

A

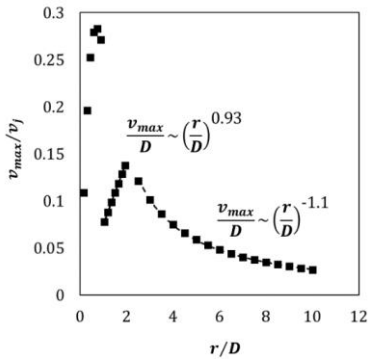

B

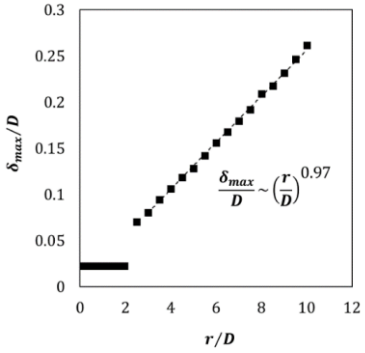

Figure 5: (**A**) Value of the maximum radial velocity inside the boundary layer at different radial locations, (**B**) Location of the radial velocity maxima from the surface at different radial locations.

III.B. Thermal and species field characterization

To further understand the parameters that affect the BF spot dimensionality, we explore the thermal and species fields in the computational domain. First, we look at the temperature field. Because the jet and ambient temperatures are the same, most of the domain is at the prescribed temperature. To further understand the evolution of the boundary layer, **Figure 6A** and **B** show the temperature profiles at different radial locations. The dimensionless temperature varies from 0.967 at the condenser surface to unity at the edge of the thermal boundary layer. From radial locations $r/D = 0.15$ to 0.9. The thermal boundary layer expands negligibly, which is shown by the small variation of the axial location at which the dimensionless temperature approaches unity in **Figure 6A**. At a radial location r/D of 1.2, the thermal boundary layer contracts back to be almost consistent with that of $r/D = 0.15$. This is consistent with our observation in **Figure 4B,** in which the momentum boundary layer at a radial location r/D of 1.2 and 0.15 are almost the same. For higher radial locations $r/D > 1.2$, the thermal boundary layer starts to grow indefinitely as depicted in **Figure 6B.**

A

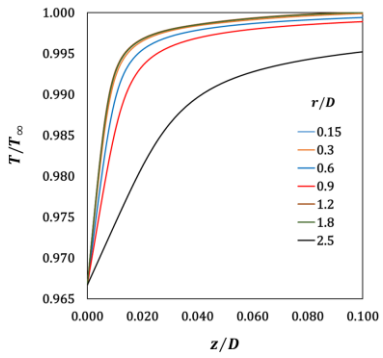

B

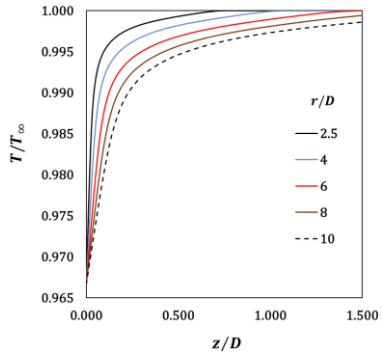

Figure 6: Distribution of temperature within the boundary layer at different radial locations (**A**) *r/D*= 0.15 − 2.5, (**B**) *r/D*= 2.5 − 10 for the case of Re = 4130 (v_j=20.24 m/s).

Figure 7A presents the contours of the water vapor mass fraction in the simulated domain. The vapor exits the tube with a uniform vapor mass fraction of 0.0022. As the jet expands in the ambient that has a lower vapor mass fraction, the vapor starts diffusing into the ambient. The maximum vapor mass fraction is always at the center of the expanding jet cone. It is observed that the vapor mass fraction value at the exit of the tube remains the maximum vapor mass fraction up to 4 diameters, and then it starts to decrease. Furthermore, as the jet impinges on the surface, the vapor is carried with the flow in the radial location, forming a concentration boundary layer on the surface.

To better understand the evolution of the concentration boundary layer, **Figure 7B** and **C** depict the dimensionless variation of the vapor mass fraction at different radial locations. The vapor mass fraction at the surface ($z/D = 0$) is observed to vary, especially after the radial locations r/D of 0.6. The variation in surface vapor mass fraction is negligible or non-present below that value which supports the work of Alshehri and Kavehpour [6].

In terms of the vapor-mass fraction profiles, we distinguish the profiles in accordance with the different regions discussed above. For radial locations r/D of 0.15 to 0.75, the vapor mass fraction varies over a large axial distance ($z/D > 1$). At a higher radial location, the boundary layer thickness decreases at r/D of 0.9, then, increases abruptly at r/D of 1.2 to coincide approximately with r/D of 0.15. This abrupt profile change is due to ambient flow circulation as the jet changes direction of flow (axial to radial). After this radial location, the vapor mass fraction boundary layer thickness decreases in self-similar profiles as depicted in **Figure 7C**.

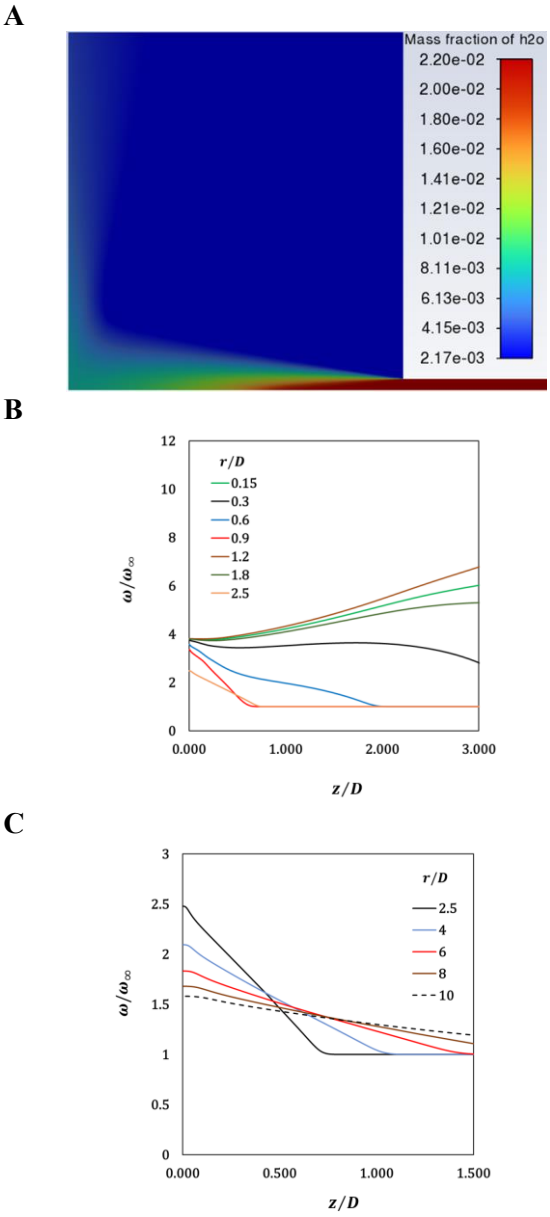

Figure 7: (**A**) Contours of water vapor mass fraction near the impingement region for the case of $Re = 4130$ (v_j=20.24 m/s), (**B** and **C**) Distribution of concentration within the boundary layer at different radial locations.

IV. Conclusions

In conclusion, this paper numerically analyzed the initial appearance of BF spots during jet impingement condensation. A jet of humidified air exiting a tube into an ambient with a lower humidity level and impinging on a condenser surface was studied. The model was validated with experimental results showing excellent agreement. To further understand the underlaying mechanisms that affect the BF spot dimensions, the flow, thermal, and concentration fields were discussed in detail. The velocity profiles at different radial locations on the condenser surface showed that there exist four different regions at which different flow characteristics can be distinguished. Furthermore, the velocity profiles are characterized by the existence of a maximum radial velocity. Variations in maximum radial velocity and axial location at which it appears were also discussed. Power-law relations were also presented to further support the semi-analytical results obtained in the literature. Finally, the temperature and vapor mass fraction profiles were discussed. This work provides a numerical tool that is useful for further investigating the condensation phenomena resulting from jet impingement of a humidified gas on a condenser surface.

Acknowledgements

The author acknowledges the support provided by the Deanship of Research Oversight and Coordination (DROC) at King Fahd University of Petroleum & Minerals (KFUPM) for partially funding this work through Project No. SR211010.

References

[1] J. Huang, J. Zhang, and L. Wang, "Review of vapor condensation heat and mass transfer in the presence of non-condensable gas," *Appl. Therm. Eng.*, vol. 89, pp. 469–484, Oct. 2015, doi: 10.1016/j.applthermaleng.2015.06.040.

[2] A. Alshehri, S. Andalib, and H. P. Kavehpour, "Numerical modeling of vapor condensation over a wide range of non-condensable gas concentrations," *Int. J. Heat Mass Transf.*, vol. 151, p. 119405, 2020.

[3] D.-Y. Ji, D. Kim, and K.-Y. Lee, "Enhancement of condensation heat transfer in the presence of non-condensable gas using steam jet method," *Int. J. Heat Mass Transf.*, vol. 130, pp. 603–612, Mar. 2019, doi: 10.1016/j.ijheatmasstransfer.2018.10.090.

[4] D.-Y. Ji, J.-W. Lee, D. Kim, W. Hwang, and K.-Y. Lee, "Effective reduction of non-condensable gas effects on condensation heat transfer: Surface modification and steam jet injection," *Appl. Therm. Eng.*, vol. 174, p. 115264, Jun. 2020, doi: 10.1016/j.applthermaleng.2020.115264.

[5] A. Alshehri, J. P. Rothstein, and H. P. Kavehpour, "Improving heat and mass transfer rates through continuous drop-wise condensation," *Sci. Rep.*, vol. 11, no. 1, p. 19636, 2021.

[6] A. Alshehri and H. P. Kavehpour, "Breath figure spot: a recovery concentration manifestation," *Int. J. Heat Mass Transf.*, vol. 172, p. 121166, 2021.

[7] Fluent ANSYS, "Ansys fluent theory guide." Ansys Inc., 2011.

[8] N. Zuckerman and N. Lior, "Jet Impingement Heat Transfer: Physics, Correlations, and Numerical Modeling," in *Advances in Heat Transfer*, Elsevier, 2006, pp. 565–631. doi: 10.1016/S0065-2717(06)39006-5.

[9] J. O. Hirschfelder, C. F. Curtiss, and R. B. Bird, "Molecular Theory of Gases and Liquids, John Wiley & Sons, New York 1954.," *N TAXMAN Phys Rev*, vol. 11, pp. 110–1235, 1958.